[2] W. Heinrich, K. Beienhoff, P. Mezzanotte, and L. Roselli, "Optimum mesh gridding for finite-difference method," *IEEE Trans. Microwave Theory Tech.*, vol. 44, pp. 1569–1573, Sept. 1996.

[3] P. Monk and E. Suli, "Error estimates for Yee's method on nonuniform grids," *IEEE Trans. Magn.*, vol. 30, pp. 3200–3203, Dec. 1994.

[4] S. Chebolu, S. Dey, R. Mittra, and J. Svigelj, "Efficient modeling of microstrip antennas using the finite-difference time-domain method," in *Advanced In Microstrip and Printed Antennas*, K. F. Lee and W. Chen, Eds.   New York: Wiley, 1997.

[5] M. W. Chevalier, R. J. Luebbers, and V. P. Cable, "FDTD local grid with material traverse," *IEEE Trans. Antennas Propagat.*, vol. 45, pp. 411–421, Mar. 1997.

[6] M. Okoniewski, E. Okoniewski, and M. A. Stuchly, "Three-dimensional subgridding algorithm for FDTD," *IEEE Trans. Antennas Propagat.*, vol. 45, pp. 422–429, Mar. 1997.

[7] G. Mur, "Absorbing boundary conditions for the finite-difference approximation of time-domain electromagnetic field equations," *IEEE Trans. Electromag. Compat.*, vol. EMC-23, pp. 377–382, Nov. 1981.

[8] J. P. Berenger, "A perfectly matched layer for the absorption of electromagnetic waves," *J. Comput. Phys.*, vol. 114, pp. 185–200, Oct. 1994.

[9] Y. Chen and R. Mittra, "Finite-difference time-domain algorithm for solving Maxwell's equations in rotationally symmetric geometries," *IEEE Trans. Microwave Theory Tech.*, vol. 44, pp. 832–839, June 1996.

[10] R. J. Luebbers, K. S. Kunz, M. Schneider, and F. Hunsberger, "A finite-difference time-domain near zone to far zone transformation," *IEEE Trans. Antennas Propagat.*, vol. 39, pp. 423–433, Apr. 1991.

[11] I. J. Craddock and C. J. Railton, "Application of the FDTD method and a full time-domain near-far transformation to the problem of radiation from a PCB," *Electron. Lett.*, vol. 29, no. 23, pp. 2017–2018, Nov. 1993.

A Modal Analysis of TEM Mode in Circular–Rectangular Coaxial Waveguides

Haiyin Wang, Ke-Li Wu, and John Litva

Abstract—A modal analysis of transverse electromagnetic (TEM) mode in a circular–rectangular coaxial waveguide is presented in this paper. The analysis is based on the modal-expansion technique. Analytic expressions for the characteristic impedance and attenuation coefficient are derived from the solution of the TEM mode. The calculated results are compared with those of the finite-element method, as well as published data. Excellent agreement is observed.

Index Terms—Coaxial waveguides, modal analysis, TEM mode.

I. INTRODUCTION

The transverse electromagnetic (TEM) mode is found to be the dominant mode in circular–rectangular (C–R) coaxial waveguides. This waveguide structure has been widely used in transitions between a circular coaxial waveguide and rectangular waveguide in various microwave systems. Many critical parameters in the RF circuit design, such as the characteristic impedance, attenuation coefficient, and Q factor can be derived by carrying out TEM-mode-based analysis. To completely understand the electromagnetic (EM) characteristics

involved, it is of primary importance to obtain the solution of the TEM mode in the C–R coaxial waveguide.

Although the finite-difference method [1] and finite-element method (FEM) offer considerable flexibility for dealing with complicated structures, their dynamic range and accuracy may be limited by numerical discretization error. Analytical solutions, on the other hand, offer the advantages of accuracy, efficiency, and an embedded physical understanding. Therefore, workers have put a great deal of effort into obtaining an analytical solution for the problem of modeling a C–R coaxial waveguide [2], [3].

Analytical expressions have been reported for deriving the characteristic impedance of a limited class of C–R coaxial waveguides. For example, the method of conformal transformation and method of images were jointly used to deduce the characteristic impedance of a C–R coaxial line [4], although the radius of the inner conductor is limited to some fraction of the size of the closure. A variational method was used to find expressions for the characteristic impedance of a "trough line" and "slab line" [5]. Similar methods were used in [6]–[8] for simulating some special cases of C–R coaxial waveguides. However, in each case, the mode field distribution was not included in the analysis. Therefore, a more general method is desired for modeling the TEM mode in a C–R coaxial waveguide.

In this paper, a modal analysis is presented to describe the TEM mode in a C–R waveguide. Instead of formulating the problem by a two-dimensional (2-D) solution as done for higher order modes [2], the solution of TEM mode is obtained by superposition of the TE and TM types of modes defined in a three-dimensional (3-D) waveguide cavity loaded with a full height conductor post. Since the resonant frequency of the cavity corresponding to the TEM mode is determined only by the given height of the resonator, the eigenvector for the TEM mode can be found without searching for the eigenvalue.

A number of practical problems are solved based on the proposed analysis. The results are compared with those calculated using the FEM and other closed-form approximations. Excellent agreement is observed in all the cases. The attenuation coefficient versus the characteristic impedance of typical coaxial waveguides is also investigated. The results reveal some useful guidelines for designing coaxial-type combline and interdigital filters.

II. THEORETICAL ANALYSIS

The TEM-mode solution of the C–R waveguide can be derived from the eigensolution of the structure of a rectangular waveguide cavity loaded with a full-height conducting post, as shown in Fig. 1(a). The discontinuity in Fig. 1(b) is divided into the following three regions:

1) rectangular region I;
2) rectangular region II;
3) cylindrical region III.

The imaginary boundary which separates the three regions is a cylindrical surface with a radius of $\rho = a$.

The longitudinal-field components in the rectangular waveguide regions can be expressed as

$$\left\{ \begin{matrix} E_z^I \\ E_z^{II} \end{matrix} \right\} = \sum_m \sum_i \left[\left\{ \begin{matrix} A_{mi}^{Ie} \\ B_{mi}^{IIe} \end{matrix} \right\} e^{-\gamma_{mi} z} - \left\{ \begin{matrix} B_{mi}^{Ie} \\ A_{mi}^{IIe} \end{matrix} \right\} e^{\gamma_{mi} z} \right] e_{zmi}^{Ie}$$

(1a)

$$\left\{ \begin{matrix} H_z^I \\ H_z^{II} \end{matrix} \right\} = \sum_m \sum_i \left[\left\{ \begin{matrix} A_{mi}^{Ih} \\ B_{mi}^{IIh} \end{matrix} \right\} e^{-\gamma_{mi} z} + \left\{ \begin{matrix} B_{mi}^{Ih} \\ A_{mi}^{IIh} \end{matrix} \right\} e^{\gamma_{mi} z} \right] h_{zmi}^{Ih}$$

(1b)
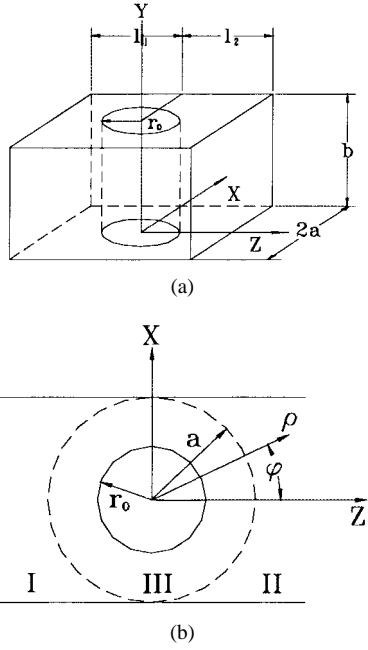
Fig. 1. (a) Waveguide cavity loaded with a full-height post. (b) Waveguide discontinuity with a full-height post.

where A_{mi}'s and B_{mi}'s are coefficients of the waveguide modes incident to and reflected from the post. e^e_{zmi} and h^h_{zmi} are z components of modal functions of electric and magnetic fields. The subscripts m and i are the mode index in x- and y-directions, and the superscripts e and h correspond to TM and TE modes with respect to the z-direction, respectively. Since the lowest resonant frequency of the TEM mode in the C–R waveguide cavity is considered, only the modal functions with $i = 1$ need to be considered. The other transverse-field components in the waveguide region can be derived straightforwardly from the z components.

The field components in the post region are described in terms of TE- and TM-type modes with respect to y direction as

$$\overline{E}_t^{III} = \sum_n \left[C^e_{n1} J_n\left(\eta^e_1 \rho\right) + D^e_{n1} Y_n\left(\eta^e_1 \rho\right) \right] \hat{e}^{IIIe}_{tn1}$$
$$+ \sum_n \left[C^h_{n1} J'_n\left(\eta^h_1 \rho\right) + D^h_{n1} Y'_n\left(\eta^h_1 \rho\right) \right] \eta^h_1 \hat{e}^{IIIh}_{tn1} \quad (2a)$$

$$E_\rho^{III} = \sum_n \left[C^e_{n1} J'_n\left(\eta^e_1 \rho\right) + D^e_{n1} Y'_n\left(\eta^e_1 \rho\right) \right] \eta^e_1 e^{IIIe}_{\rho n1}$$
$$+ \sum_n \left[C^h_{n1} J_n\left(\eta^h_1 \rho\right) + D^h_{n1} Y_n\left(\eta^h_1 \rho\right) \right] \hat{e}^{IIIh}_{\rho n1} \quad (2b)$$

$$\overline{H}_t^{III} = \sum_n \left[C^e_{n1} J'_n\left(\eta^e_1 \rho\right) + D^e_{n1} Y'_n\left(\eta^e_1 \rho\right) \right] \eta^e_1 \hat{h}^{IIIe}_{tn1}$$
$$+ \sum_n \left[C^h_{n1} J_n\left(\eta^h_1 \rho\right) + D^h_{n1} Y_n\left(\eta^h_1 \rho\right) \right] \hat{h}^{IIIh}_{tn1} \quad (2c)$$

with the transverse modal functions defined as

$$\hat{e}^{IIIe}_{tn1}$$
$$= \hat{y} \left\{ \begin{array}{c} \sin(n\phi) \\ \cos(n\phi) \end{array} \right\} \cos(k_{y1} y) - \hat{\phi} \left\{ \begin{array}{c} \cos(n\phi) \\ -\sin(n\phi) \end{array} \right\} \frac{n k_{y1}}{\rho \eta^{e2}_1} \sin(k_{y1} y) \quad (3a)$$

$$j\omega\mu \hat{h}^{IIIh}_{tn1}$$
$$= \hat{y} \left\{ \begin{array}{c} \cos(n\phi) \\ -\sin(n\phi) \end{array} \right\} \sin(k_{y1} y) - \hat{\phi} \left\{ \begin{array}{c} \sin(n\phi) \\ \cos(n\phi) \end{array} \right\} \frac{n k_{y1}}{\rho \eta^{h2}_1} \cos(k_{y1} y) \quad (3b)$$

where $\eta^2_1 = k^2_0 - k^2_{y1}$, $k_{y1} = \frac{\pi}{b}$, and k_0 are the wavenumbers in free space.

To satisfy the boundary condition that the tangential components of the field in the waveguide and post regions are continuous across the imaginary boundary $\rho = a$, one needs to take inner products of an electric-field continuity equation with $\hat{h}^{IIIe}_{tn1}$ and $\hat{h}^{IIIh}_{tn1}$, and magnetic field continuity equation with $\hat{e}^{IIIe}_{tn1}$ and $\hat{e}^{IIIh}_{tn1}$ respectively, yielding

$$[\mathbf{W}] \begin{bmatrix} \mathbf{C}^e \\ \mathbf{D}^e \\ \mathbf{C}^h \\ \mathbf{D}^h \end{bmatrix} = \{\mathbf{0}\} \quad (4)$$

and

$$[\mathbf{Q}] \begin{bmatrix} \mathbf{C}^e \\ \mathbf{D}^e \\ \mathbf{C}^h \\ \mathbf{D}^h \end{bmatrix} = \begin{bmatrix} \mathbf{p}_{11} & \mathbf{p}_{12} & \cdots & \mathbf{p}_{18} \\ \mathbf{p}_{21} & \mathbf{p}_{22} & \cdots & \mathbf{p}_{28} \\ \mathbf{p}_{31} & \mathbf{p}_{32} & \cdots & \mathbf{p}_{38} \\ \mathbf{p}_{41} & \mathbf{p}_{42} & \cdots & \mathbf{p}_{48} \end{bmatrix} \begin{bmatrix} \mathbf{A}^{Ie} \\ \mathbf{A}^{Ih} \\ \mathbf{A}^{IIe} \\ \mathbf{A}^{IIh} \\ \mathbf{B}^{Ie} \\ \mathbf{B}^{Ih} \\ \mathbf{B}^{IIe} \\ \mathbf{B}^{IIh} \end{bmatrix} \quad (5)$$

where the elements in the $\mathbf{W}$ and $\mathbf{Q}$ matrices contain only the Bessel functions of the first and second kinds, and the elements of $\mathbf{p}_{ij}$ involve the inner product $\langle \hat{e}^{IIIq}_{tn1}, e^{\pm\gamma_m z} \hat{h}^{I,IIq}_{tm1} \rangle_{\rho=a}$ or $\langle e^{\pm\gamma_m z} \hat{e}^{I,IIq}_{tm1}, \hat{h}^{IIIq}_{tn1} \rangle_{\rho=a}$ with definition

$$\langle \hat{e}, \hat{h} \rangle_{\rho=a} = \iint_S (\hat{e} \times \hat{h})_{\rho=a} \cdot \hat{n}\, dS$$
$$= \int_0^b dy \int_{\phi_1}^{\phi_2} (e_\phi h_y - e_y h_\phi)_{\rho=a}\, a\, d\phi.$$

By combining (4) and (5), one can easily get

$$[\mathbf{W}] \begin{Bmatrix} \mathbf{C}^e \\ \mathbf{D}^e \\ \mathbf{C}^h \\ \mathbf{D}^h \end{Bmatrix} = [\mathbf{W}][\mathbf{Q}]^{-1}[\mathbf{P}] \begin{Bmatrix} \mathbf{A} \\ \mathbf{B} \end{Bmatrix} = [\mathbf{W}][\mathbf{X}_A \quad \mathbf{X}_B] \begin{Bmatrix} \mathbf{A} \\ \mathbf{B} \end{Bmatrix} = \{\mathbf{0}\}$$
$$(6)$$

where $\mathbf{X}_A$ corresponds to the wave incident to the post region and $\mathbf{X}_B$ corresponds to the wave reflected from the post region. From the definition of the general scattering matrix, (6) can be rearranged as

$$\{\mathbf{B}\} = [\mathbf{S}]\{\mathbf{A}\} = -([\mathbf{W}][\mathbf{X}_B])^{-1}[\mathbf{W}][\mathbf{X}_A]\{\mathbf{A}\} \quad (7)$$

with respect to the reference plane at the center of the post. By applying the boundary condition of the two conducting planes at the ends of the cavity, one can obtain the matrix expression given by

$$\left\{ \begin{bmatrix} \mathbf{D}_1 & \mathbf{0} \\ \mathbf{0} & \mathbf{D}_2 \end{bmatrix} [\mathbf{S}] \begin{bmatrix} \mathbf{D}_1 & \mathbf{0} \\ \mathbf{0} & \mathbf{D}_2 \end{bmatrix} + [\mathbf{I}] \right\} \{\mathbf{A}'\} = \{\mathbf{0}\} \quad (8)$$

where the submatrix $\mathbf{D}_k$ is a diagonal transmission matrix with $d_{ii} = e^{-\gamma_i l_k}$, $[\mathbf{I}]$ is the identity matrix, and $\{\mathbf{A}'\}$ is the coefficient vector of the incident wave with shifted reference planes. The characteristic equation $\det([\mathbf{D}][\mathbf{S}][\mathbf{D}] + [\mathbf{I}]) = 0$ must be satisfied to ensure existence of the eigensolution of (8).

Intuitively, it is known that the lowest resonant mode of the cavity corresponds to the TEM mode in the transverse direction with the wavelength equal to twice the height of the cavity. In other words, the eigenvector $\{\mathbf{A}'\}$ can be determined from (8) with the known resonant frequency. Once the eigenfield distributions are found, the characteristic impedance for a C–R coaxial waveguide can be obtained by

$$Z = \frac{V}{I} = \frac{\int_{r_0}^a E_\rho^{III}(\phi = \pi/2)\, d\rho}{\oint H_\phi^{III}(\rho = \rho_0)\rho_0\, d\phi} \quad r_0 \le \rho_0 \le a \quad (9)$$

where V is the voltage between the inner and outer conductors and I is the total current flowing on the inner conductor. To calculate the voltage V, the electric field E_ρ needs to be integrated from the inner conductor to the outer conductor along any path. A judicious choice is the path along $\phi = \pi/2$

$$\int_{r_0}^{a} E_\rho^{III}(\phi = \pi/2)\, d\rho = \sum_{n=0}^{N} \left(V_n^e + V_n^h\right) \qquad (10)$$

with V_n^e and V_n^h shown in (11a) and (11b) at the bottom of the page. The analytic expression for the total current flowing on the inner conductor is given by

$$\oint H_\phi^{III} \rho_0\, d\phi = \left[C_{01}^e J'\left(\eta_1^e \rho_0\right) + D_{01}^e Y_0'\left(\eta_1^e \rho_0\right)\right] \frac{k_0^2}{\eta_1^2} 2\pi \cos\left(\frac{\pi}{b}y_0\right)\rho_0. \qquad (12)$$

From the definition of the attenuation coefficient due to the finite conductivity, we have

$$\alpha = \frac{P_c}{2P_0} = \frac{R_s \int_{C_1+C_2} \bar{H}\cdot\bar{H}^*\, dl}{2\int_{r_0}^{a} E_\rho^{III}\left(\phi = \frac{\pi}{2}\right) d\rho \oint H_\phi^{III} \rho_0\, d\phi} \qquad (13)$$

where P_c is the power loss per unit length of the waveguide, P_0 is the power flowing down the transmission line, R_s is the surface resistance of the conductors, C_1 and C_2 represent the integration paths over the inner and outer conductor boundaries, and $\bar{H}$ is the tangential component of the magnetic field.

III. NUMERICAL RESULTS AND DISCUSSION

To verify the accuracy of the solution, the field distribution in a C–R coaxial waveguide and related parameters are calculated. The resonant frequency chosen for the computation is 9.8357 GHz, which means that the corresponding half-wavelength is equal to the resonator length of 0.6 in. It is found that when four TE and four TM symmetric modes in the rectangular waveguide and eight TE and eight TM symmetric modes in the cylindrical region are used, the numerically found resonant frequency is accurate to four decimal places.

Fig. 2 shows the characteristic impedance of a C–R coaxial waveguide versus the ratio of r/a. The result is compared with that obtained using a commercial finite-element package (Ansoft's HFSS). Fig. 3 represents a comparison of the calculated value using a proposed formulation for the characteristic impedance of a slab line with the results reported in [5]. In both cases, excellent agreement is obtained.

The even- and odd-mode impedance Z_e and Z_o of a multiple inner conductor structure versus the ratio of r/a is presented in Fig. 4. Perfect electric walls are used at the two sides of the resonator for calculating Z_o, and perfect magnetic walls are used for calculating Z_e. Excellent agreement is observed between the calculated results and those published in [9]. The Z_e and Z_o of the multiple inner
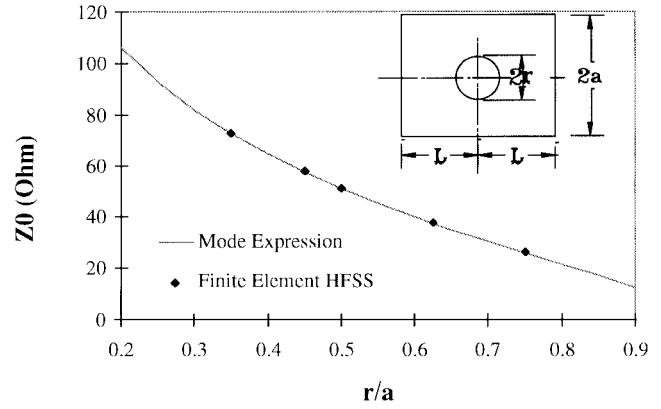
Fig. 2. The characteristic impedance of a C–R coaxial waveguide versus r/a, where $L/a = 1.25$ in and $a = 0.5$ in.
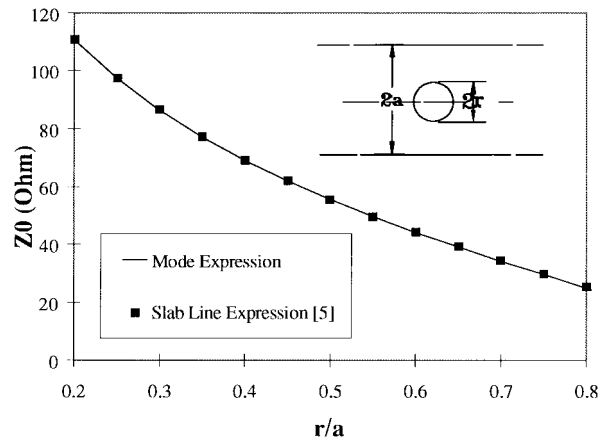
Fig. 3. The characteristic impedance of a slab line versus r/a.

conductor coaxial line are important parameters in designing coaxial-line interdigital filters.

It is worth mentioning that in all the examples calculated in this paper, the value of the impedance increases as r decreases or l_1 and l_2 increase. When l_1 and l_2 are greater than $3a$, the value of the impedance tends to be a constant.

The attenuation due to the conductor loss versus the characteristic impedance for different ratios of L/a is plotted in Fig. 5. The attenuation achieves the minimum value as the impedance varies from 70 to 80 Ω. The attenuation of a circular coaxial waveguide is also plotted in the same figure. The inner conductor of the circular coaxial waveguide has the same radius as that of the C–R waveguides. The radius of outer conductor is chosen such that the outer conductor of the circular coaxial waveguide covers the same area as that of the circular–square coaxial waveguide ($L/a = 1$). The minimum

$$V_n^e = \left\{C_{n1}^e\left[J_n\left(\eta_1^e a\right) - J_n\left(\eta_1^e r_0\right)\right] + D_{n1}^e\left[Y_n\left(\eta_1^e a\right) - Y_n\left(\eta_1^e r_0\right)\right]\right\}\begin{Bmatrix}\sin(n\phi)\\\cos(n\phi)\end{Bmatrix}\frac{(-\pi)}{b\eta_1^{e2}}\sin\left(\frac{\pi}{b}y_0\right) \qquad (11a)$$

$$V_n^h = C_{n1}^h\begin{Bmatrix} J_n\left(\eta_1^h a\right) - J_n\left(\eta_1^h r_0\right) - 2\sum_{k=1}^{n/2}\left[J_{2k}\left(\eta_1^h a\right) - J_{2k}\left(\eta_1^h r_0\right)\right] - J_0\left(\eta_1^h a\right) + J_0\left(\eta_1^h r_0\right)\\ n = 0, 2, 4, \cdots\\ J_n\left(\eta_1^h a\right) - J_n\left(\eta_1^h r_0\right) - 2\sum_{k=0}^{(n-1)/2}\left[J_{2k}\left(\eta_1^h a\right) - J_{2k}\left(\eta_1^h r_0\right)\right] + \int_{r_0}^{a} J_0\left(\eta_1^h r\right)\eta_1^h\, dr\\ n = 1, 3, 5, \cdots\end{Bmatrix}\begin{Bmatrix}\sin(n\phi)\\\cos(n\phi)\end{Bmatrix}\frac{1}{\eta_1^{h2}}\sin\left(\frac{\pi}{b}y_0\right)$$

$$+ D_{n1}^h\begin{Bmatrix} Y_n\left(\eta_1^h a\right) - Y_n\left(\eta_1^h r_0\right) - 2\sum_{k=1}^{n/2}\left[Y_{2k}\left(\eta_1^h a\right) - Y_{2k}\left(\eta_1^h r_0\right)\right] - Y_0\left(\eta_1^h a\right) + Y_0\left(\eta_1^h r_0\right)\\ n = 0, 2, 4, \cdots\\ Y_n\left(\eta_1^h a\right) - Y_n\left(\eta_1^h r_0\right) - 2\sum_{k=0}^{(n-1)/2}\left[Y_{2k}\left(\eta_1^h a\right) - Y_{2k}\left(\eta_1^h r_0\right)\right] + \int_{r_0}^{a} Y_0\left(\eta_1^h r\right)\eta_1^h\, dr\\ n = 1, 3, 5, \cdots\end{Bmatrix}\begin{Bmatrix}\sin(n\phi)\\\cos(n\phi)\end{Bmatrix}\frac{1}{\eta_1^{h2}}\sin\left(\frac{\pi}{b}y_0\right) \qquad (11b)$$
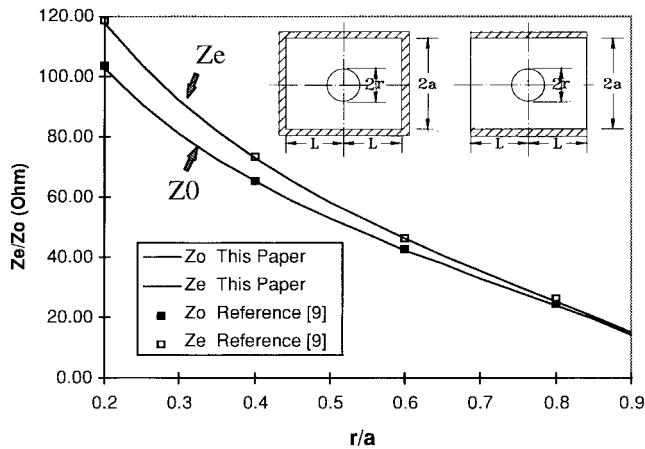
Fig. 4. The even- and odd-mode impedance of the C–R waveguide with a multiple inner conductors versus r/a, where $L/a = 0.9 + r/a$.
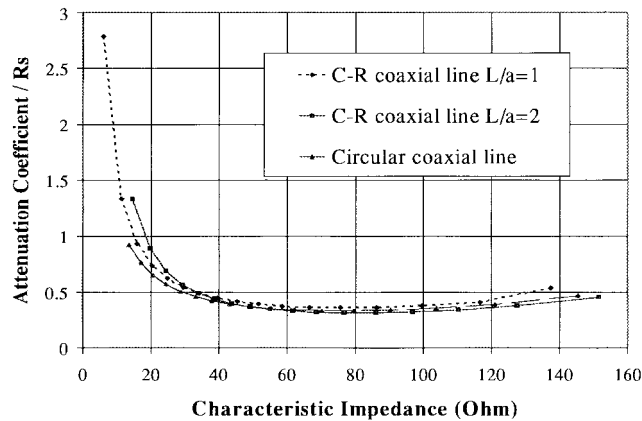
Fig. 5. The attenuation coefficient of a C–R waveguide versus characteristic impedance with $a = 0.5$ in.

attenuation is achieved around 75 Ω in the case of the circular coaxial waveguide. It can be seen that it is a good approximation to estimate the conductor loss of C–R waveguides using the formulation for circular coaxial lines.

IV. Conclusion

A modal solution of the TEM mode in the C–R coaxial waveguide is presented in this paper. The general expression for the characteristic impedance is derived. Three typical C–R waveguide examples are examined using the proposed method. The results are compared with those obtained either by a finite-element software package or by other methods described in the referenced literature. Excellent agreement is observed in all cases. The attenuation coefficient in the waveguides can also be calculated using the proposed formulation. An optimal dimension aspect ratio for the minimum power loss provides a guideline in designing combline type of filters. The solution of asymmetric C–R waveguide can be similarly obtained using the addition theorems of Bessel functions.

References

[1] C. T. Carson, "The numerical solution of TEM mode transmission lines with curved boundaries," *IEEE Trans. Microwave Theory Tech.*, vol. MTT-15, pp. 269–270, Apr. 1967.

[2] H. Wang, K.-L. Wu, and J. Litva, "The higher order modal characteristics of circular–rectangular coaxial waveguides," *IEEE Trans. Microwave Theory Tech.*, vol. 45, pp. 414–419, Mar. 1997.

[3] A. S. Omar and K. Schuenemann, "Application of the generalized spectral-domain technique to the analysis of rectangular waveguides with rectangular and circular metal inserts," *IEEE Trans. Microwave Theory Tech.*, vol. 39, pp. 944–952, June 1991.

[4] S. Frankel, "Characteristic impedance of parallel wires in rectangular troughs," *Proc. IRE*, vol. 30, pp. 182–190, Apr. 1942.

[5] R. M. Chisholm, "The characteristic impedance of trough and slab lines," *IRE Trans. Microwave Theory Tech.*, vol. MTT-4, pp. 166–173, July 1956.

[6] W. Lin, "A critical study of the coaxial transmission line utilizing conductors of both circular and square cross section," *IEEE Trans. Microwave Theory Tech.*, vol. MTT-30, pp. 1981–1988, Nov. 1982.

[7] H. A. Wheeler, "Transmission-line properties of a round wire in a polygon shield," *IEEE Trans. Microwave Theory Tech.*, vol. MTT-27, pp. 717–721, Aug. 1979.

[8] E. G. Cristal, "Characteristic impedance of coaxial lines of circular inner and rectangular outer conductors," *Proc. IEEE*, vol. 52, pp. 1265–1266, Oct. 1964.

[9] ——, "Coupled circular cylindrical rods between parallel ground planes," *IEEE Trans. Microwave Theory Tech.*, vol. MTT-12, pp. 428–439, July 1964.

Improving Amplifier Stability Through Resistive Loading Below the Operating Frequency

Sun-Wook Kim, Ik-Soo Chang, Won-Tae Kang, and In-Pyo Kyung

Abstract—A new design method for a stable RF amplifier using a broad-band-matched 3-dB coupled line is proposed in this paper. The proposed broad-band matching circuit consists of lossless matching circuits at operating frequency band and resistive matching circuits at frequencies below the operating band. This design method improves the stability of the amplifier and is suitable for the design of a power amplifier and multistage amplifier. When applying this proposed method to a design of a two-stage power amplifier for personal communication systems, measured results show 18.0-dB gain and 9-W (39.5-dBm) output power.

Index Terms—Amplifier, broad-band matching, power amplifier, stability.

I. Introduction

Generally, if an amplifier is designed with its matching circuits having bandpass characteristics like those of a π- or L-type network etc., it has narrow-band matching characteristics at input and output only within the operating frequency band. At frequencies below the operating band (in this paper, dc to 1840-MHz band), it is difficult to achieve good input, output matches, and good stability so that the amplifier can oscillate by the noise or the unstable characteristics of the transistor itself [2].

Thereby, in this paper, broad-band matching circuits are designed using resistive decoupling circuits, impedance converters, and 3-dB coupled lines. As an application of this matching circuit, a stable RF high-power amplifier for a personal communication system (PCS)